Charge doping versus impurity scattering in chemically substituted iron pnictides

Alexander Herbig,[1] Rolf Heid,[1] and Jörg Schmalian[1,2]

[1]*Institut für Festkörperphysik, Karlsruher Institut für Technologie, 76021 Karlsruhe, Germany*

[2]*Institut für Theorie der Kondensierten Materie, Karlsruher Institut für Technologie, 76131 Karlsruhe, Germany*

(Received 23 October 2015; revised manuscript received 2 August 2016; published 14 September 2016)

To reveal the relative importance of charge doping and defect scattering in substitutionally modified 122 iron pnictides, we perform a systematic first-principles study on selected bands at the Fermi level. Disorder effects are induced by various substitutions using an orbital-based coherent potential approximation. Pronounced level shifts of individual bands suggest that transition-metal substitutions introduce mobile charge carriers into the system. However, important deviations from such a rigid-band scenario as well as spectral broadenings due to impurity scattering correlate with the band character. Finally, a T-matrix analysis exhibits a larger intraband than interband scattering consistent with an s^{+-} pairing state. Comparing different substitutions reveals an increase of pair breaking along the transition-metal series.

DOI: 10.1103/PhysRevB.94.094512

I. INTRODUCTION

Chemical substitution is an important tuning parameter which governs the phase diagram and thus the onset of superconductivity in the various iron pnictide superconductors. Despite intensive experimental and theoretical work on a variety of different families of these compounds, the role of substitutional disorder is still under debate. In particular the substitution of Fe by other $3d$ transition metals (TM) in the 122 family such as $BaFe_2As_2$ has been discussed controversially. Macroscopic measurements over a range of compositions [1] suggest that the number of extra d electrons at the TM site is the decisive quantity which determines the shape of the superconducting dome for TM $\in$ {Co,Ni}. Such a rigid-band-shift scenario is also compatible with changes of Fermi surfaces as observed in angle-resolved photoemission spectroscopy (ARPES) [2,3]. On the other hand, x-ray absorption measurements (x-ray absorption near-edge structure, near-edge x-ray-absorption fine structure) [4,5] see at best a small change of valence at the Fe atom induced by TM substitution, which challenges the view of a rigid-band shift. This finding is also consistent with the dependence of the Néel temperature on chemical substitution reported in [1]. From the viewpoint of electronic structure calculations this dichotomy between localized extra electrons and doping into conduction bands was first addressed by standard supercell calculations [6] and their combination with Wannier-function-based averaging techniques [7–9]. More recently, effective medium approaches, which can handle arbitrary impurity concentrations, have been used to study the effect of substitutional disorder on band structure and Fermi surface topology [10,11]. Nevertheless, a systematic first-principles investigation of different substitutions on the behavior of electronic quasiparticles is still lacking.

A further aspect of substitutional disorder is its impact on the superconducting state. It is widely accepted that these systems are unconventional superconductors in which impurity scattering is important for Cooper pair breaking [12–19]. For example, the popular s^{+-} pairing state would be more susceptible to interband scattering [20] than the more conventional s^{++} state. Thus, knowledge of the band-resolved scattering rates induced by the different substituents can shed light on the symmetry of possible superconducting gap functions.

In this paper we performed electronic structure calculations of substitutionally disordered iron-based systems to address these topics. We focus on disorder-induced level shifts and spectral broadenings due to impurity scattering on individual hole and electron bands at the Fermi level. We systematically investigated the $Ba(Fe_{1-x}TM_x)_2As_2$ series where TM $\in$ {Mn, Co, Ni, Cu, Zn, Pd, Pt} as well as the $Ba_{1-x}K_xFe_2As_2$ and the $BaFe_2(As_{1-x}P_x)_2$ systems at impurity concentrations $x < 0.1$. Additionally, we analyzed the impact of these substitutions on intra- and interband scattering in the limit of small impurity concentrations.

Our major findings are as follows: (i) Impurity substitution leads to both level shifts and spectral broadening; that is, TM substitutions simultaneously supply mobile carriers and act as scattering centers. (ii) The magnitude of level shifts and degree of spectral broadenings due to impurity scattering depend sensitively on orbital composition and the specific location in momentum space of the states. This reveals an ability to affect and pin the much discussed orbital fluctuations in the iron-based systems. (iii) A stronger intraband scattering on hole bands dominating the transport properties and a weaker interband scattering between electron and hole bands render the s^{+-} pairing state [21,22] comparatively robust.

II. THEORY

In our non-spin-polarized electronic structure calculations the substitutional disorder was treated within Blackman, Esterling, and Berk's [23] extension of the coherent potential approximation (BEB-CPA) [24,25], which is an effective-medium method dedicated to the treatment of arbitrary impurity concentrations. Unlike the conventional CPA, the BEB-CPA additionally allows us to incorporate off-diagonal disorder effects in the hopping terms, essentially accounting for disorder-induced changes in the hybridization which are the key effect of structural distortions. Following earlier work [26], the charge-self-consistent BEB-CPA was implemented using a nonorthogonal set of atom-centered basis functions which were obtained from fits to *ab initio* band structures of the parent compound $BaFe_2As_2$ and the respective substitutional

end-member, for example, $BaTM_2As_2$, by means of density functional theory (DFT), which also provided the required potentials to calculate the BEB-CPA Hamiltonian. We used nine local basis functions up to an orbital angular momentum of $l = 2$ for each atomic species. All calculations were done in the tetragonal high-temperature phase of the stoichiometric $BaFe_2As_2$ with the structural parameters given in [27] using the 2-Fe and 2-As unit cell. The crystal structure was not changed with impurity concentration x in order to separate disorder from structural effects. Additional test calculations for 10% Co as well as 7% Ni substitution performed with experimental structure parameters after [28] showed no considerable changes to the results presented below. The DFT calculations were performed within the mixed-basis-pseudopotential approach (MBPP code) [29,30] applying the local-density approximation (LDA) [31]. The Brillouin-zone integration was performed on a $8 \times 8 \times 4$ Monkhorst-Pack [32] $\mathbf{k}$ mesh. We used norm-conserving pseudopotentials constructed after Vanderbilt [33] together with local d-type functions for Fe or TM and plane waves up to a cutoff energy of 22 Ry.

For TM substitutions we find modifications of the density of states (DOS) similar to those in previous Wannier-function-based calculations [7]. In particular, only at Zn substitution does a localized state form at 7 eV below the Fermi level. To obtain a deeper insight into effects of disorder on selected bands near the Fermi level we considered the Bloch spectral function

$$A(\mathbf{k},\omega) = -\frac{1}{\pi}\mathrm{Im}\mathrm{Tr}[S(\mathbf{k})\Gamma(\mathbf{k},\omega)],$$

where Γ is the BEB-CPA effective-medium Green's function, S is the overlap matrix, and the trace is taken over local basis indices. In Fig. 1(a) $A(\mathbf{k},\omega)$ is plotted in false color over the energy along a path in $\mathbf{k}$ space for disordered $Ba(Fe_{0.9}Ni_{0.1})_2As_2$ together with the band structure of the parent compound. It contains all information about the effects of disorder on the band structure, in particular shifts with respect to the parent compound and $\mathbf{k}$-dependent spectral widths in energy. $A(\mathbf{k},\omega)$ exhibits a multipeak structure, which, for example, can be seen in Fig. 1(b) as a solid black line at a fixed $\mathbf{k}$ point next to the X-point indicated by the vertical red line in Fig. 1(a). To be able to perform a quantitative analysis of disorder effects on selected bands we projected the Green's function on the eigenvectors $\mathbf{c}_n(\mathbf{k})$ of the Hamiltonian of the parent compound

$$G_n(\mathbf{k},\omega) \equiv \sum_{i,j\in\text{parent}} c^*_{n,i}(\mathbf{k})[S(\mathbf{k})\Gamma(\mathbf{k},\omega)S(\mathbf{k})]_{i,j}c_{n,j}(\mathbf{k}), \quad (1)$$

where n is a band index and i,j are local basis indices. This is only valid in the limit of small x because Γ is given in the full Hilbert space of the disordered system while the sum in Eq. (1) only runs over the subspace of the parent compound. Some of these band-projected spectral functions are shown in Fig. 1(b), and each of them consists of a single peak with a well-defined position and spectral width even in regions where bands hybridize. The sum over these four bands (dashed gray line) agrees with the total spectral function, indicating that this decomposition works well even for 10% substitution.

From this analysis we can extract the level shift of any selected band by comparing the projected spectral function

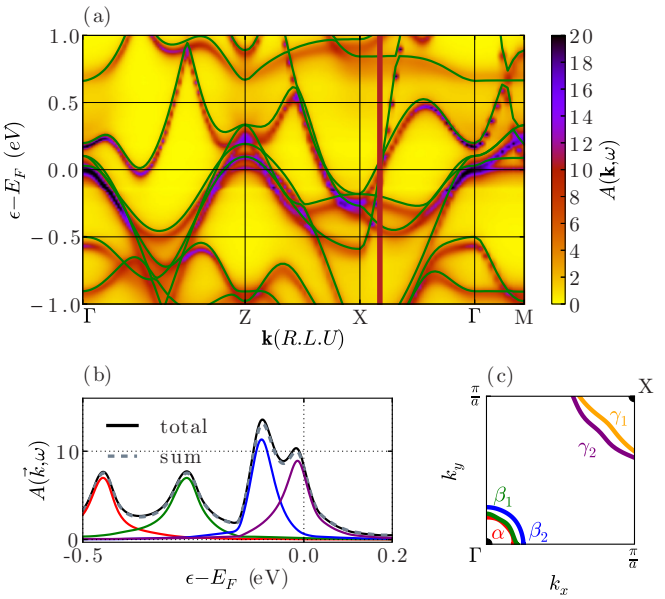

FIG. 1. (a) Bloch spectral function of disordered $Ba(Fe_{0.9}Ni_{0.1})_2As_2$ together with band structure of the parent compound (green solid lines), (b) Bloch spectral function of $Ba(Fe_{0.9}Ni_{0.1})_2As_2$ at a single $\mathbf{k}$ point [vertical red line in (a)] together with projections (red, green, blue, and purple) on bands of the parent compound and sum over all bands, and (c) the Fermi surface of the parent compound in the $(\mathbf{k}_x,\mathbf{k}_y)$ plane at $\mathbf{k}_z = 0$.

of the disordered system with that of the parent compound. Concerning the broadening, we assumed a Lorentzian shape for G_n which has to be evaluated at a slightly complex frequency $\omega + i\delta$,

$$G_n(\mathbf{k},\omega) = \frac{1}{\omega + i\delta - \epsilon_n(\mathbf{k}) - \Sigma_n}, \quad (2)$$

where $\epsilon_n(\mathbf{k})$ is the band dispersion of the parent compound, anticipating the level shifts and broadenings to be the real and imaginary parts of the band self-energy Σ_n, respectively. From evaluation of Eq. (2) at the poles the spectral width is given by $\mathrm{Im}[1/G_n(\omega_0)]$ provided the peak position ω_0 is known.

III. RESULTS

In Fig. 1(c) a cross section of the Fermi surface in the $(\mathbf{k}_x,\mathbf{k}_y)$ plane at $\mathbf{k}_z = 0$ is shown for the parent compound; it essentially consists of three holelike cylinders (α, β_1, β_2) around the center of the Brillouin zone (Γ point) and two electronlike cylinders (γ_1, γ_2) around the zone corner (X point). By calculating level shifts and spectral broadenings for these five bands along the Γ-Z and the X-Γ directions, we empirically found in good approximation $\mathrm{Re}\Sigma_n \propto x$ and $\mathrm{Im}\Sigma_n \propto x$ for $x \leqslant 0.1$. Therefore, to obtain general trends in a compact way, we restrict ourselves in the following to the discussion of the slopes of these quantities depending on the substituent.

In Fig. 2 the slopes of the level shifts $d\mathrm{Re}\Sigma_n/dx$ for the five bands are plotted for various substitutions, including K for Ba and P for As. These level shifts were taken at the Fermi wave vector $\mathbf{k}_F$ of the disordered system. We also

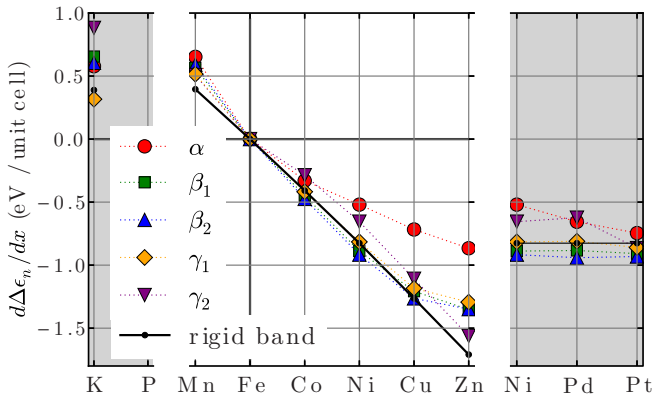

FIG. 2. Slopes of level shifts $d\mathrm{Re}\Sigma_n/dx$ plotted over the substituent (points) together with rigid band shift (solid line). Besides the TM substitution series for Fe, substitutions of K for Ba and P for As are shown on the left.

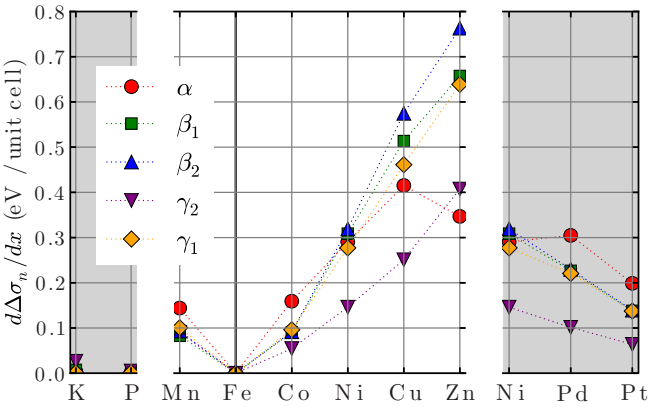

FIG. 3. Slopes of the band broadenings $d\mathrm{Im}\Sigma_n/dx$ plotted over the substituent. Besides the TM substitution series for Fe, substitutions of K for Ba and P for As are shown on the left.

calculated the respective rigid-band shift by integrating the density of states of the parent compound and adjusting the Fermi level to the expected number of extra charge carriers to be doped into the system, which is shown as solid black line. In general our band-selective level shifts follow the trend of the rigid-band shift. The deviations from the rigid-band shift get more pronounced as the difference $|\Delta_{\mathrm{val}}| = |z_{\mathrm{val}}(\mathrm{impurity}) - z_{\mathrm{val}}(\mathrm{parent})|$ between the valence electron numbers of the parent compound and the impurity increases but decrease as the extent of the d orbitals increases in the case of Pd and Pt substitution. On the electron-doped side for Ni, Cu, and Zn substitution, the electron band γ_2 and, especially, the hole band α deviate more strongly from the rigid-band shift than the remaining bands. These two bands have a similar orbital character; they are mainly $d_{x^2-y^2}$ bands, where x and y are oriented along the projections of Fe-As bonds into the Fe planes. Overall, this is consistent with the experimentally established [1] dependence of the superconducting transition temperature on the number of extra d electrons, provided that the $d_{x^2-y^2}$ bands do not significantly contribute to the pairing state. In contrast, we find no substantial changes either in the local charge densities at the TM sites or in the species and angular momentum resolved electron numbers due to Co substitution. This finding shows that the doping scenario of itinerant carriers is not necessarily a contradiction to an unchanged local charge.

What, in addition, can we learn from the disorder-induced lifetime effects? Figure 3 shows how the slopes of the respective band broadenings $d\mathrm{Im}\Sigma_n/dx$ taken at the Fermi wave vector $\mathbf{k}_F$ of the disordered system behave under different substitutions. This analysis exhibits the general feature that only TM substitutions in the iron planes lead to substantial broadening effects, whereas out-of-plane substitutions (Ba for K and As for P) hardly show any broadenings. This agrees with the fact that the major contribution to the band structure near the Fermi level stems from Fe d states. The TM substitutions additionally show a trend similar to that already shown by the level shifts: an increase in $|\Delta_{\mathrm{val}}|$ causes enhanced broadenings. This makes sense because in this context we also find an increase in the $l = 2$ contributions to the scattering potential upon moving through the TM series. Similar to the level shifts, the broadenings become less pronounced as the extent of the d orbitals increases. Again the broadenings are band selective. In particular, hole bands β_1, β_2 and electron band γ_1, being of similar orbital character d_{xz}, d_{yz}, exhibit the same trend, while among the remaining states with $d_{x^2-y^2}$ character in particular the electron band γ_2 shows considerably less broadening.

What do these impurity scattering effects imply for superconductivity in the Ba-122 systems? Among various proposals concerning the order parameter, the most promising candidate turned out to be the s^{+-} state [21,22], where the gap obeying s-wave symmetry changes sign between hole and electron pockets on the Fermi surface [Fig. 1(c)]. The important difference in the s^{+-} scenario compared to conventional s-wave pairing is the distinction between intraband and interband scattering. While in conventional superconductors all scattering processes on nonmagnetic impurities are not pair breaking due to Anderson's theorem [34], interband scattering rapidly suppresses T_c in an s^{+-} superconductor. At the same time, intraband scattering is irrelevant for pair breaking but determines the residual resistivity [20]. The impurity scattering effects we considered above reveal the joint impact of intra- and interband scattering on a band. In order to obtain details about scattering between different bands we consider the T matrix of inserting a single impurity into the disordered crystal in the dilute limit

$$T_{m,n}(\mathbf{k},\mathbf{k}') = \langle m,\mathbf{k}|V + V\Gamma(E_F)V + \cdots|n,\mathbf{k}'\rangle, \qquad (3)$$

where we used the charge-self-consistent effective-medium Green's function $\Gamma(E_F)$ and the difference between the impurity block and the parent block of the charge-self-consistent on-site Hamiltonian for the impurity potential V. This T matrix includes repeated scatterings at the same impurity up to infinite order. Via Fermi's golden rule we calculated the scattering rates

$$w_{m,n} = 2\pi x|\mathcal{T}_{m,n}|^2\nu_n(E_F), \qquad (4)$$

where $\nu_n(E_F)$ is the partial DOS of band n at the Fermi level and $\mathcal{T}$ is the $\mathbf{k}$ average of T over all initial and final points to get overall trends. We additionally averaged over the two outer hole bands $\langle\beta_1,\beta_2\rangle \to \beta$ and over the two electron bands $\langle\gamma_1,\gamma_2\rangle \to \gamma$ because their $\mathbf{k}$-space anisotropy mutually

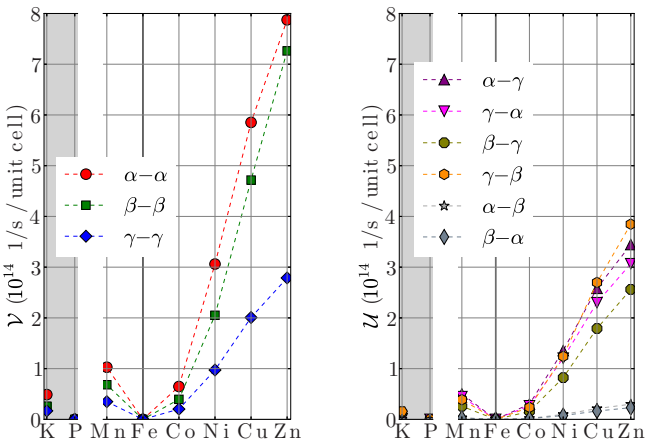

FIG. 4. Concentration normalized intraband $\mathcal{V}$ and interband $\mathcal{U}$ scattering rates obtained from the single-impurity T matrix in the dilute limit.

cancels and divided the results by x. These concentration normalized intraband $\mathcal{V}$ and interband $\mathcal{U}$ scattering rates between the three effective bands are shown in Fig. 4. We find that the intraband scattering rates inside the hole bands are the largest, whereas the electron intraband and electron-hole interband scattering rates are smaller by a factor of 2. The interband scattering between hole bands α and β is negligible. This behavior is universal for all TM substitutions and indicates that an s^{+-} state can exist in these systems together with considerable impurity scattering because the latter is dominated by intraband scattering, which is not relevant for pair breaking. For Co substitution transport measurements [35] reveal a larger scattering of hole carriers which is consistent with our findings because transport properties are predominantly intraband phenomena. In addition, the sum over all intraband scattering rates is of the same order of magnitude as the experimental transport scattering rates compiled in [36].

Furthermore the scattering rates show the same trend as the band broadenings already did: they grow for increasing $|\Delta_{\text{val}}|$ and are only relevant for TM substitution. Under the assumption of s^{+-} superconductivity this tells us that Co substitution is more strongly pair breaking than K, and for TM substitution the pair-breaking strength increases with Δ_{val}. Clearly, this can be connected with experimental facts because at optimal doping for the critical temperatures among the different substitutions it holds that $T_c(\text{K}) > T_c(\text{Co}) > T_c(\text{Ni}) > T_c(\text{Cu})$. Mn substitution does not follow this trend due to our above-mentioned non-spin-polarized calculations, which shows the importance of a local magnetic moment for impurity scattering in the case of Mn in contrast to the other substitutions.

IV. CONCLUSIONS

In conclusion, we have presented a systematic *ab initio* study of disorder effects for a variety of substitutions in the Ba-122 compound. For TM substitution, shifts of individual bands at the Fermi level are, to first approximation, compatible with the picture of adding charge carriers to the system together with no considerable changes in the local charge densities. However, there are deviations from this rigid band behavior which, like the spectral broadenings, are connected to the orbital composition of the band and the substitutional site. An analysis distinguishing intra- and interband scattering in the dilute limit substantiates the robustness of the proposed s^{+-} pairing state. Among different substitutions this analysis indicates growing pair breaking with an increasing number of d electrons for TM substitution, in qualitative agreement with experiment.

ACKNOWLEDGMENTS

We acknowledge R. Eder, K. Grube, F. Hardy, M. Hoyer, and H. v. Löhneysen for fruitful discussions and suggestions. All plots within this paper have been generated by MATPLOTLIB [37], an open source project.

[1] P. C. Canfield, S. L. Bud'ko, N. Ni, J. Q. Yan, and A. Kracher, Phys. Rev. B **80**, 060501 (2009).
[2] C. Liu, T. Kondo, R. Fernandes, A. Palczewski, E. Mun, N. Ni, A. Thaler, A. Bostwick, E. Rothenberg, J. Schmalian, S. Bud'ko, P. Canfield, and A. Kaminski, Nat. Phys. **6**, 419 (2010).
[3] M. Neupane, P. Richard, Y.-M. Xu, K. Nakayama, T. Sato, T. Takahashi, A. V. Federov, G. Xu, X. Dai, Z. Fang, Z. Wang, G.-F. Chen, N.-L. Wang, H.-H. Wen, and H. Ding, Phys. Rev. B **83**, 094522 (2011).
[4] E. M. Bittar, C. Adriano, T. M. Garitezi, P. F. S. Rosa, L. Mendonça Ferreira, F. Garcia, G. d. M. Azevedo, P. G. Pagliuso, and E. Granado, Phys. Rev. Lett. **107**, 267402 (2011).
[5] M. Merz, F. Eilers, T. Wolf, P. Nagel, H. v. Löhneysen, and S. Schuppler, Phys. Rev. B **86**, 104503 (2012).
[6] H. Wadati, I. Elfimov, and G. A. Sawatzky, Phys. Rev. Lett. **105**, 157004 (2010).
[7] T. Berlijn, C.-H. Lin, W. Garber, and W. Ku, Phys. Rev. Lett. **108**, 207003 (2012).
[8] T. Berlijn, P. J. Hirschfeld, and W. Ku, Phys. Rev. Lett. **109**, 147003 (2012).
[9] L. Wang, T. Berlijn, Y. Wang, C.-H. Lin, P. J. Hirschfeld, and W. Ku, Phys. Rev. Lett. **110**, 037001 (2013).
[10] S. N. Khan, A. Alam, and D. D. Johnson, Phys. Rev. B **89**, 205121 (2014).
[11] G. Derondeau, S. Polesya, S. Mankovsky, H. Ebert, and J. Minár, Phys. Rev. B **90**, 184509 (2014).
[12] R. Balian and N. R. Werthamer, Phys. Rev. **131**, 1553 (1963).
[13] J. Annett, N. Goldenfeld, and S. R. Renn, Phys. Rev. B **43**, 2778 (1991).
[14] A. A. Golubov and I. I. Mazin, Phys. Rev. B **55**, 15146 (1997).
[15] A. P. Mackenzie and Y. Maeno, Rev. Mod. Phys. **75**, 657 (2003).
[16] A. V. Balatsky, I. Vekhter, and J.-X. Zhu, Rev. Mod. Phys. **78**, 373 (2006).
[17] H. Alloul, J. Bobroff, M. Gabay, and P. J. Hirschfeld, Rev. Mod. Phys. **81**, 45 (2009).

[18] V. G. Kogan, Phys. Rev. B **80**, 214532 (2009).
[19] P. J. Hirschfeld, M. M. Korshunov, and I. I. Mazin, Rep. Prog. Phys. **74**, 124508 (2011).
[20] A. B. Vorontsov, M. G. Vavilov, and A. V. Chubukov, Phys. Rev. B **79**, 140507 (2009).
[21] J. Zhang, R. Sknepnek, R. M. Fernandes, and J. Schmalian, Phys. Rev. B **79**, 220502 (2009).
[22] R. Sknepnek, G. Samolyuk, Y.-B. Lee, and J. Schmalian, Phys. Rev. B **79**, 054511 (2009).
[23] J. A. Blackman, D. M. Esterling, and N. F. Berk, Phys. Rev. B **4**, 2412 (1971).
[24] D. W. Taylor, Phys. Rev. **156**, 1017 (1967).
[25] P. Soven, Phys. Rev. **156**, 809 (1967).
[26] K. Koepernik, B. Velický, R. Hayn, and H. Eschrig, Phys. Rev. B **55**, 5717 (1997).
[27] S. Drotziger, P. Schweiss, K. Grube, T. Wolf, P. Adelmann, C. Meingast, and H. v. Löhneysen, J. Phys. Soc. Jpn. **79**, 124705 (2010).
[28] M. Merz, P. Schweiss, P. Nagel, M.-J. Huang, R. Eder, T. Wolf, H. von Löhneysen, and S. Schuppler, J. Phys. Soc. Jpn. **85**, 044707 (2016).
[29] B. Meyer, F. Lechermann, C. Elsässer, and M. Fähnle, FORTRAN90 program for mixed-basis pseudopotential calculations for crystals (Max-Planck-Institut für Metallforschung, Stuttgart) (unpublished).
[30] S. G. Louie, K.-M. Ho, and M. L. Cohen, Phys. Rev. B **19**, 1774 (1979).
[31] J. P. Perdew and Y. Wang, Phys. Rev. B **45**, 13244 (1992).
[32] H. J. Monkhorst and J. D. Pack, Phys. Rev. B **13**, 5188 (1976).
[33] D. Vanderbilt, Phys. Rev. B **32**, 8412 (1985).
[34] P. Anderson, J. Phys. Chem. Solids **11**, 26 (1959).
[35] F. Rullier-Albenque, D. Colson, A. Forget, and H. Alloul, Phys. Rev. Lett. **103**, 057001 (2009).
[36] K. Kirshenbaum, S. R. Saha, S. Ziemak, T. Drye, and J. Paglione, Phys. Rev. B **86**, 140505 (2012).
[37] J. D. Hunter, Comput. Sci. Eng. **9**, 90 (2007).